Magnetic Microhelix Coil Structures

Elliot J. Smith,[1] Denys Makarov,[1,*] Samuel Sanchez,[1] Vladimir M. Fomin,[1] and Oliver G. Schmidt[1,2,†]

[1]*Institute for Integrative Nanosciences, IFW Dresden, Helmholtzstrasse 20, 01069 Dresden, Germany*

[2]*Material Systems for Nanoelectronics, Chemnitz University of Technology, Reichenhainer Strasse 70, 09107 Chemnitz, Germany*

(Received 21 April 2011; published 26 August 2011)

Together with the well-known ferro- and antiferromagnetic ordering, nature has created a variety of complex helical magnetic configurations. Here, we design and investigate three-dimensional microhelix coil structures that are radial-, corkscrew-, and hollow-bar-magnetized. The magnetization configurations of the differently magnetized coils are experimentally revealed by probing their specific dynamic response to an external magnetic field. Helix coils offer an opportunity to realize microscale geometries of the magnetic toroidal moment, observed so far only in bulk multiferroic materials.

DOI: 10.1103/PhysRevLett.107.097204 PACS numbers: 75.70.Cn, 68.35.Gy

The impact of topology on electromagnetic properties of physical objects with complex magnetic configurations allows for new effects to be observed [1,2], for example, the recently discovered topological Hall effect [3] in helimagnetic materials [4]. Helimagnetic materials are characterized by a gradual spatial tilt of adjacent discrete spin moments to form Skyrmions or helical spin structures. This class of materials reveals metamagnetic transitions [5], which have been analyzed theoretically [6]. However, only a limited number of experimental works have been reported [7,8], since a material must exhibit extraordinary properties for the stabilization of helimagnetism. For instance, a real-space manifestation of Skyrmions has been discovered in a material with cubic but noncentrosymmetric structure [7].

An alternative approach to create complex magnetic patterns relies on a continuous distribution of the macroscopic magnetic moment. Such geometries can be prepared by using micro- and nanofabrication [9,10]. For instance, by creating a lateral confinement of a thin ferromagnetic layer in the shape of a disk, an interesting topological object, identified as a magnetic vortex, has been observed [11,12]. Recent advances in nanofabrication have also led to experimental detection of magnetic monopoles [13].

Here we create and investigate complex helimagnetic-like configurations, namely, hollow-bar-, corkscrew-, and radial-magnetized 3D microhelix coils [Figs. 1(a)–1(c)]. The fabrication starts with a planar strip geometry possessing a well-defined easy axis of magnetization either in-plane or out-of-plane. If the magnetic moment is oriented in-plane, orthogonal to the strip axis, the coiling process results in a hollow-bar-magnetized structure [Fig. 1(a)]. If, instead, the magnetic moment is oriented in-plane, parallel to the strip axis, a corkscrew-magnetized helix coil structure is expected [Fig. 1(b)]. Alternatively, if the easy axis of magnetization of the strip is pointing out-of-plane, a radial-magnetized helix coil geometry is realized [Fig. 1(c)]. We focus on fabrication of the magnetic microhelix coils possessing as many as three distinct magnetic configurations. These patterns are then physically probed by dynamical magnetometry using parametric magnetic excitation.

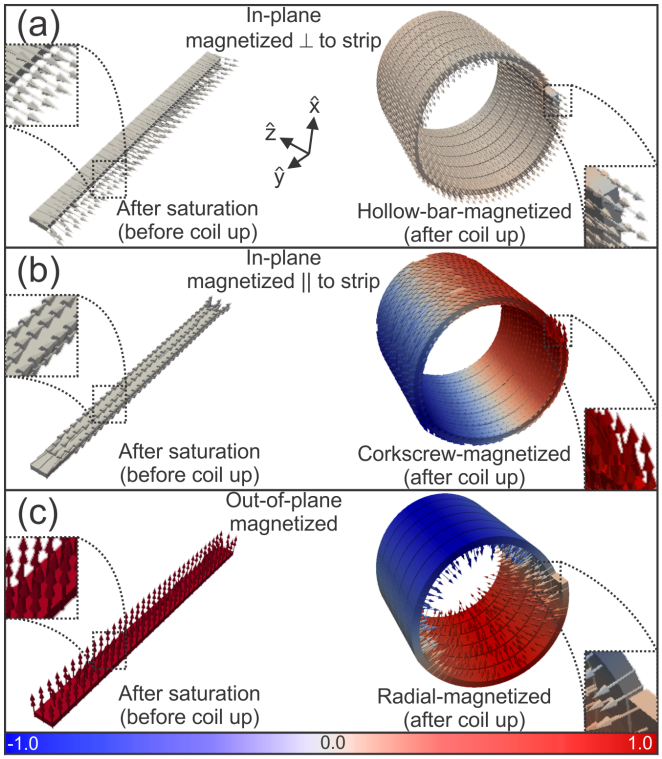

FIG. 1 (color online). Obtainable magnetization orientations of a helix coil. Micromagnetic simulations carried out on planar and coiled-up magnetic strips: (a) Initial magnetization is in-plane, perpendicular-to-strip (left); hollow-bar-magnetized helix coils can be created (right). (b) Initial magnetization is in-plane, parallel-to-strip (left), results in a corkscrew-magnetized coil (right). (c) An out-of-plane magnetized strip (left) assembles into a radial-magnetized coil (right). Simulation details are given in [15].

The fabrication of 3D microhelix coils relies on a straightforward process: We first define SU8 strips [1 mm × 7 μm × (2–10 μm)/$L \times W \times H$], by means of photolithography. Next we deposit an "active" magnetic layer. The layer makeup of the devices for the out-of-plane and in-plane magnetized active layer is detailed in Fig. 2(a). For the magnetic film with an in-plane magnetic easy axis, a 20-nm-thick Co layer was chosen to create either corkscrew-magnetized or hollow-bar-magnetized helix coil structures [Figs. 1(a) and 1(b)]. The radial-magnetized coils were made by using an active magnetic $[\mathrm{Co}(0.4\ \mathrm{nm})/\mathrm{Pt}(0.6\ \mathrm{nm})]_5$ multilayer stack with a well-defined out-of-plane easy axis of magnetization [14]. In addition, a nonmagnetic reference sample consisting of a $[\mathrm{Cu}(0.4\ \mathrm{nm})/\mathrm{Pt}(0.6\ \mathrm{nm})]_5$ multilayer was also prepared. For film properties, see [15].

Deposition of the active layer onto SU8 leads to a differential strain throughout the structure. Such strain engineering is a widely used technique [16–19] and was recently applied in order to fabricate and control magnetic swimmers [18,20]. A delamination process is then performed by placing the sample into *N*-methyl-2-pyrrolidone, and the strips spontaneously form into the 3D helix coils [Fig. 2(c) and video 5 [15]]. During the delamination process [Fig. 2(b)], the strained strip (the active layer and SU8) relaxes, causing the strips to coil up (video 5 [15]). The radius of the coil is dependent on the thickness of the SU8 resist and thus can be tailored by varying the thickness of SU8. In particular, when the thickness of the SU8 is 6.2 μm, the resulting radius of the coil is 35 μm (50 μm in length). The self-assembly process usually results in the coils detaching from the substrate. Given that the coils are untethered, the substrate below the coil can be exchanged. This makes it possible to study the effect the substrate has on a coil's motion.

One physical attribute of the system is friction, which plays a large role determining whether or not the coil dynamics result in forward propagation or stationary rotation. For the scope of this Letter, substrates with magnetic films and glass were used. If using a magnetic substrate, there is an additional attraction of the coil to the magnetized substrate. When a coil structure has a thin (< 5.5 μm) SU8 layer, this magnetic attraction is strong enough to prevent motion of the coil. In contrast, when the coil is positioned on the glass substrate, the friction is

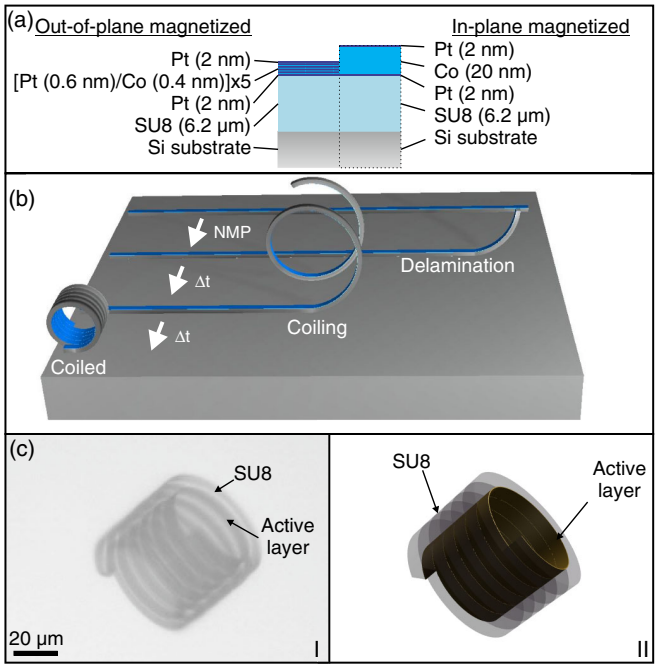

FIG. 2 (color online). Makeup and assembly of differently magnetized hybrid coils. (a) Composition of the different layer stacks for a hard out-of-plane or in-plane magnetized active layer. (b) Self-assembled coiling process: A photolithographic step defines the SU8 pattern. The active layer is deposited on top of this. The SU8 is delaminated from the substrate in *N*-methyl-2-pyrrolidone, causing the gradient strain between the SU8 and active layer to lead to a roll-up. (c) An optical image (i) and artist rendition (ii) of a hybrid helix coil with an SU8 organic outer layer and an inorganic magnetic (active) inner layer.

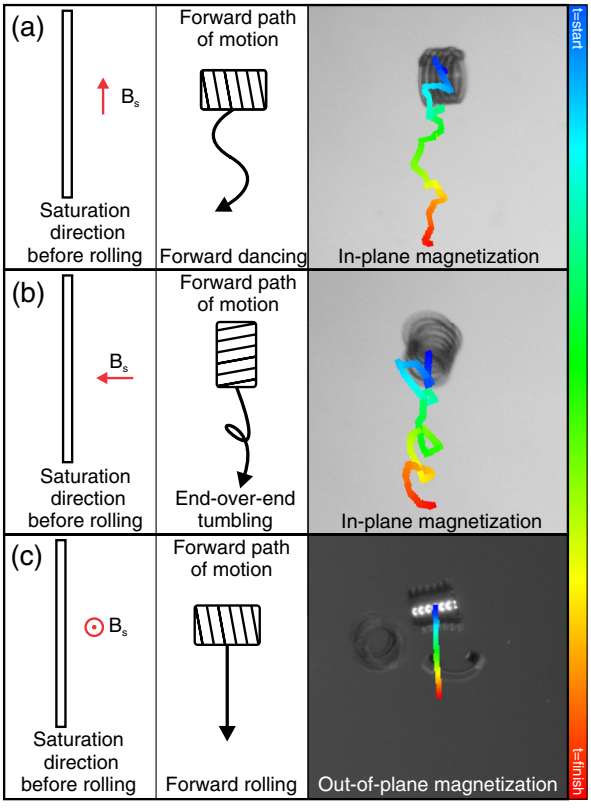

FIG. 3 (color online). Tracking of coil trajectory vs magnetized film orientation. (a) Coils with in-plane magnetized films in the parallel-to-strip direction exhibit forward dancing motion. (b) Coils with in-plane magnetized films in the perpendicular-to-strip direction exhibit end-over-end tumbling. (c) Straight and deterministic forward motion of coils with out-of-plane magnetized films.

lowered and the coil responds to an external magnetic field through stationary, rotationlike motion. Therefore, the thickness of the SU8 layer has to be optimized in order to achieve controlled directed propulsion of the coil, which is crucial for applications like fuel-free cargo delivery. While it is challenging to directly measure the magnetic configuration of the coils, we reveal the magnetic state by probing the response of the coils to an alternating external magnetic field. The experimental setup for the investigation of the motion of the coils is shown in [15], the right side of Supplemental Fig. 3. Because of the spatial position of the permanent magnet, the external magnetic field exerted on a coil has a rather complex profile (Supplemental Fig. 3 [15]) resulting in a parametric excitation which determines the specific dynamics of the coils. The main source of force acting on the coil originates from this magnetic torque, while the magnetic field gradient has only a minor influence on the motion [15].

Tracking of the forward progression of coils with different magnetization alignments [Figs. 1(a)–1(c)] is performed as shown in Fig. 3 and videos 1–3 [15]. Each type of magnetic coil responds uniquely to the external magnetic field; in short, corkscrew-magnetized helix coils exhibit a forward dancing motion [Fig. 3(a) and video 2 [15]]. The hollow-bar-magnetized coils perform end-over-end tumbling because the effective magnetic moment is similar to a hollow-bar magnet [Fig. 3(b) and video 3 [15]]. The forward motion of the radial-magnetized coil is found to be directionally deterministic [Fig. 3(c) and video 1 [15]]. Although the self-assembled coiling process works for all deposited active films, the directionally deterministic motion is exceptional for the radial-magnetized coil; therefore, we focus on the dynamics of this geometry and work with a substrate on which the coils have minimal friction. This allows us to study the rotational aspect of the coils' motion.

Because of its symmetry, a radial-magnetized cylinder is expected to be magnetically compensated. However, a coil structure has an uncompensated magnetic moment as a result of the windings at either end (Fig. 4 and Supplemental Fig. 1 [15]). The uncompensated moment of the coil tries to align to the orientation of the external magnetic field. Given that the coercive field of the film (≈ 22 mT) is much larger than the external magnetic field (≤ 10 mT), a switching of the magnetic moment orientation in the $[Co/Pt]_5$ multilayer stack is unlikely. Therefore alignment of the uncompensated magnetic moment is

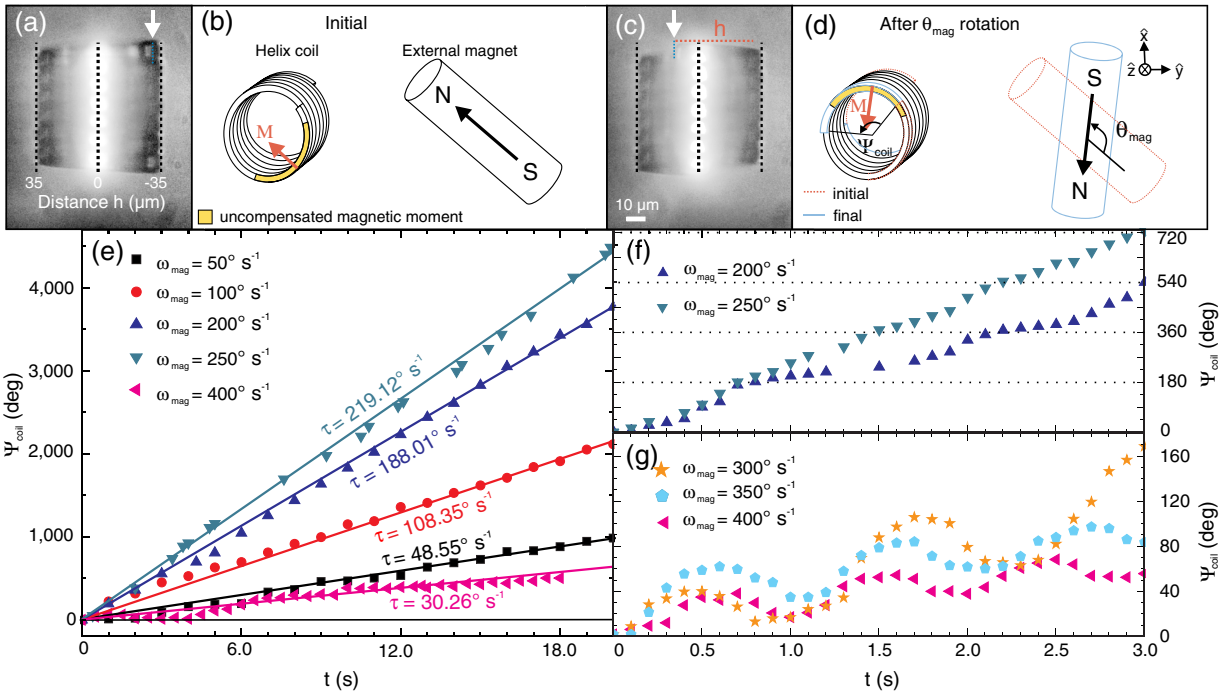

FIG. 4 (color online). Response of radial-magnetized coils to an alternating external magnetic field. (a),(c) Optical microscopy images revealing the rotation of the coil over approximately 120° when the permanent magnet is rotated the same number of degrees. A tracking of either end of the coil can be made (red dotted line). The axis of the coil is oriented perpendicular to the field lines of the permanent magnet. (b),(d) Corresponding schematic images showing the coil's rotation angle Ψ_{coil} after a rotation of the permanent magnet over the angle θ_{mag}. The uncompensated magnetic moment is indicated in yellow. (e) Time evolution of the coil's rotation angle Ψ_{coil} for various rotation speeds of the permanent magnet ω_{mag}. The slope τ of each curve reveals the average rotation speed of the coil for a corresponding ω_{mag}. When $\omega_{\text{mag}} \geq \omega_{\text{mag}}^{\text{transition}}$ (here $250^\circ\ \text{s}^{-1} < \omega_{\text{mag}}^{\text{transition}} < 300^\circ\ \text{s}^{-1}$), the average rotational velocity of the coil drops off. (f) A close-up view of two full rotations of the coil for values of $\omega_{\text{mag}} < \omega_{\text{mag}}^{\text{transition}}$ shows that the motion of the coil is rotative but not linear. (g) A close-up view for $\omega_{\text{mag}} > \omega_{\text{mag}}^{\text{transition}}$ illustrates an oscillatorylike rotative motion of the coil.

possible only through a physical rotation of the coil around $\hat{z}$ (Fig. 4). We can track one end of a coil in comparison to the rotation of the external magnetic field [schematized in Figs. 4(b) and 4(d)].

The external magnet was rotated at various angular velocities ω_{mag}, and the responding angular position of the coil, Ψ_{coil}, was recorded [Figs. 4(e)–4(g)]. The slopes of the data fit, τ, are used to derive an average rotational angular velocity of the coil. Yet, due to the nonlinear nature of the motion, τ does not represent the real full angular velocity of the coil. The average rotational angular velocity increases with increasing ω_{mag}. However, as ω_{mag} increases, τ begins to lag behind and eventually drops off above a certain critical frequency region $\omega_{\mathrm{mag}}^{\mathrm{transition}}$. This behavior is characteristic of all coils investigated, and $\omega_{\mathrm{mag}}^{\mathrm{transition}}$ is found to be dependent on the coil dimensions. For the coil under discussion, a critical frequency region of $250^\circ\ \mathrm{s}^{-1} < \omega_{\mathrm{mag}}^{\mathrm{transition}} < 300^\circ\ \mathrm{s}^{-1}$ was measured, described as a transition from rotational to oscillatorylike rotative (OLR) motion. If a close-up (3 s time lapse) is made for $\omega_{\mathrm{mag}} = 150^\circ$ and $200^\circ\ \mathrm{s}^{-1}$ [Fig. 4(f)], one can see that Ψ_{coil} vs t has an average positive slope. When $\omega_{\mathrm{mag}} > \omega_{\mathrm{mag}}^{\mathrm{transition}}$, OLR motion of the coil occurs, which is composed of oscillations superimposed over the rotative motion [Fig. 4(g)]. For the linear velocities observed in these rotational experiments ($\sim 2\ \mu\mathrm{m/s}$, which is typical for coils with a minimal friction coefficient with the substrate), the Reynolds number [21] can be estimated to be approximately 7×10^{-5}. Similar systems working at low Reynolds numbers have been theoretically described by balancing their hydrodynamic and magnetic torques [22], which is a standard method to reveal the dynamics of objects moving in viscous fluids [20] at a small scale. A theoretical explanation of the experimentally detected coil dynamics will be published elsewhere.

In summary, we have designed microhelix coils with different magnetic states: radial-, corkscrew-, and hollow-bar-magnetized, which are experimentally verified by exploring the response of the coils to an alternating external magnetic field. The continuously distributed macroscopic magnetic moment of the microhelix coils resembles that of the discrete spin patterns of helimagnetic materials. This approach opens the possibility to investigate the complex magnetic transitions, characteristic of helimagnetic materials, for the first time at the micrometer scale. Furthermore, the coil structures are of interest as a microscale geometrical realization of the so-called magnetic toroidal moment [23], thus allowing for experimental investigations on this novel type of multiferroic material. In addition, due to their particular deterministic motion, the radial-magnetized helix coils offer foreseeable practical applications in the realm of microrobotics and roving sensors. In this respect, future potential applications, such as in biomedicine, require fuel-free environments. Recently, the motion of flexible DNA-linked assemblies of paramagnetic microparticles and magnetically controlled motion of efficient artificial flagella consisting of helical tails was demonstrated [20,24]. It should be noted that the presented approach to fabricate microhelix coils is rather universal and is not limited to magnetic materials.

The authors thank C. Ortix and J. van den Brink for fruitful discussions and C. Krien for layer deposition. This work was supported by MURI, AFOSR Grant No. FA9550-09-1-0550, Volkswagen Foundation (I/84 072), and DFG Research Unit 1713.

*To whom all correspondence should be addressed.
d.makarov@ifw-dresden.de
†o.schmidt@ifw-dresden.de

[1] Y. Taguchi, Y. Oohara, H. Yoshizawa, N. Nagaosa, and Y. Tokura, Science **291**, 2573 (2001).
[2] P. Bruno, V. K. Dugaev, and M. Taillefumier, Phys. Rev. Lett. **93**, 096806 (2004).
[3] M. Lee, W. Kang, Y. Onose, Y. Tokura, and N. P. Ong, Phys. Rev. Lett. **102**, 186601 (2009).
[4] X. Z. Yu *et al.*, Nature (London) **465**, 901 (2010).
[5] L. Udvardi, S. Khmelevskyi, L. Szunyogh, P. Mohn, and P. Weinberger, Phys. Rev. B **73**, 104446 (2006).
[6] U. K. Rößler, A. N. Bogdanov, and C. Pfleiderer, Nature (London) **442**, 797 (2006).
[7] M. Uchida, Y. Onose, Y. Matsui, and Y. Tokura, Science **311**, 359 (2006).
[8] S. Mühlbauer *et al.*, Science **323**, 915 (2009).
[9] M. Boncheva *et al.*, Proc. Natl. Acad. Sci. U.S.A. **102**, 3924 (2005).
[10] R. J. Jackman, S. T. Brittain, A. Adams, M. G. Prentiss, and G. M. Whitesides, Science **280**, 2089 (1998).
[11] T. Shinjo, T. Okuno, R. Hassdorf, K. Shigeto, and T. Ono, Science **289**, 930 (2000).
[12] B. Pigeau *et al.*, Nature Phys. **7**, 26 (2010).
[13] E. Mengotti *et al.*, Nature Phys. **7**, 68 (2010).
[14] P. F. Carcia, A. D. Meinhaldt, and A. Suna, Appl. Phys. Lett. **47**, 178 (1985).
[15] See Supplemental Material at http://link.aps.org/supplemental/10.1103/PhysRevLett.107.097204 for magnetic film properties, the experimental setup, the micromagnetic simulations, and videos revealing the coil dynamics.
[16] O. G. Schmidt and K. Eberl, Nature (London) **410**, 168 (2001).
[17] V. Luchnikov, O. Sydorenko, and M. Stamm, Adv. Mater. **17**, 1177 (2005).
[18] Y. F. Mei *et al.*, Adv. Mater. **20**, 4085 (2008).
[19] F. Balhorn *et al.*, Phys. Rev. Lett. **104**, 037205 (2010).
[20] L. Zhang *et al.*, Appl. Phys. Lett. **94**, 064107 (2009).
[21] E. M. Purcell, Am. J. Phys. **45**, 3 (1977).
[22] A. Ranzoni *et al.*, Lab Chip **10**, 179 (2010).
[23] C. Ederer and N. A. Spaldin, Phys. Rev. B **76**, 214404 (2007).
[24] R. Dreyfus *et al.*, Nature (London) **437**, 862 (2005).